13th World Conference on Earthquake Engineering
Vancouver, B.C., Canada
August 1-6, 2004
Paper No. 669

Experimental Study for Multiple Friction Pendulum System

C. S. Tsai[1], Tsu-Cheng Chiang[2], Bo-Jen Chen[3]

SUMMARY

The Multiple Friction Pendulum (MFPS) which is a kind of base isolation systems has been developed in this study to provide as a means for protecting structures from earthquake damage. The doubled concave sliding interfaces, articulated slider and advanced Teflon composite are very different from the traditional FPS device. The development of the MFPS isolator is aimed at improving the durability and upgrading the earthquake-proof capability of the traditional FPS isolator under near-source excitations and strong ground motions with long predominant periods. This study mainly consists of the component tests of the advanced Teflon composite, the prototype MFPS isolator and the shaking table test of a full-scale structure with MFPS isolators. The experimental results of component test show that the new lubricant material possesses low friction coefficients and excellent durability under high compressive loading, and over 2400 cyclic loadings without any sign of deterioration. Furthermore, the MFPS isolator has been equipped beneath each column of the three-story structure at the National Center for Research on Earthquake Engineering to demonstrate its seismic resistance capability. The experimental results from the shaking table tests of the 1940 El Centro, 1995 Kobe, 1999 Chi-Chi and 331 Hua-Lien earthquakes show that the proposed isolator can reduce the undesirable seismic responses of the structure by lengthening the fundamental period of the structure during earthquakes, and that the MFPS isolator provides provide the structure with excellent isolation function under the far- and near-source excitations and strong ground motions with long predominant periods. From these experimental observations, it can be concluded that the proposed MFPS isolator is a powerful tool for enhancing the seismic-resistibility of structures.

INTRODUCTION

Base isolation is a promising technique for controlling the seismic response of structures during earthquake motions. Among the base isolation devices, the FPS isolator proposed by V. A. Zayas [1] has been proven as an effective tool for isolating seismic transmitted energy through comprehensive experimental and numerical studies [1-7]. However, the experimental

---

[1]Professor, Department of Civil Engineering, Feng Chia University, 407 Taichung, Taiwan, R. O. C.
[2]Ph. D. Candidate, Graduate Institute of Civil and Hydraulic Engineering, Feng Chia University, 407 Taichung, Taiwan, R. O. C.
[3]Assistant Research Fellow, Department of Research and Development, Earthquake Proof System, Inc, Taichung,Taiwan, R. O. C.

efforts in those studies have merely focused on the effectiveness of the scaled FPS devices under earthquake ground motions away from active faults. In recent years, there have been significant studies on the efficiency of the base isolator as subjected to near-fault ground motions [8]. It is suggested that the earthquake with long predominant periods always give the base-isolated structure a significant impact. In view of this, an advanced isolator called the “Multiple Friction Pendulum System” (MFPS) has been proposed in this study [9, 10]. As shown in Fig. 1, the MFPS consists of two spherical concave surfaces and a special articulated slider which can be another sliding surface. Based on this special design, the displacement capacity is twice of the FPS isolator with a single sliding surface. Moreover, the fundamental frequency is lower than that of the FPS due to the series connection of the doubled sliding surfaces. Hence, the proposed device can be given as a more effective tool to reduce the seismic response of structures even subjected to the earthquakes with long predominant periods. The contents of this study are mainly grouped into four parts which are: (i) component tests for the advanced Teflon composite, (ii) component tests for a full-scale MFPS isolator, (iii) shaking table tests for a full scale steel structure with MFPS isolators, and [iv] numerical analyses by using the mathematical model proposed in this study. The results from component tests and shaking table tests show that the proposed device is a promising one to upgrade the seismic resistibility of the structures. Furthermore, the numerical study show that the formulations presented in this study can well predict the behavior of the structure isolated with MFPS isolators.

COMPONENT TESTS FOR ADVANCED TEFLON COMPOSITE AND FULL SCALE MFPS ISOLATOR

The durability of the Teflon composite, which is an important key to decide whether the bearing is capable of sustaining high compressive stress and thousands of cyclic loadings without any deterioration. The mechanical behavior of the Teflon composite is very complicate and some results on experiments and theories has been proposed by Mokha et al. [11] and Constantinou et al. [12]. In this study, an advanced Teflon composite with new formula has been developed as the lubricant material on the sliding surfaces of the MFPS base isolator. As shown in Fig. 2, the steel plates were coated with the advanced Teflon composite and the high density chrome respectively to rub against each other. During the tests, the axially compressive stresses imposing at the interface are 41.342Mpa, 55.133Mpa, 68.925Mpa, 82.700Mpa and 96.476Mpa, respectively. The amplitude of the cyclic horizontal displacement is set to be 10mm, and the tests were performed at the frequencies of 0.01Hz, 0.05Hz, 0.1Hz, 0.2Hz, 0.4Hz, 0.6Hz, 0.8Hz, 1Hz, 1.2Hz, 1.4Hz, 1.6Hz, 1.8Hz and 2Hz, respectively. The shape of the displacement cycles during the tests are ramp waves. Fig. 3 shows the recorded friction coefficient of the advanced Teflon composite under an axial stress of 41.342Mpa and horizontally reversal loadings. It is evidently demonstrated from the figure that the coefficients of friction are almost identical under the same sliding velocity. Therefore, the durability of the proposed material can be guaranteed throughout these tests. The friction coefficients of the Teflon composite under different axial stresses are given in Fig. 4. It is evidently shown from the figure that the mechanical behavior of the advanced Teflon composite is very similar to that proposed by Mokha et al. [11]. The friction coefficient approaches a constant value while the sliding velocity is higher than a certain value, however, the friction coefficient gradually decreases as increasing the axially compressive stress.

In order to assess the feasibility of the MFPS isolator for the practical use and its behavior under an axial loads in the practical situation, full scale MFPS base isolator tests were conducted under an axial load of 900tons and horizontally cyclic loadings in this study. Fig. 5 shows the dimensions of the base isolator and the outline of the biaxial machine. The radius of curvature of the polished-steel sliding interface is 2.236m, and the diameter of the articulated slider is 600mm. During the tests, the horizontal sliding velocity had been set to be 0.423cm/sec. In the experimental studies, 228 cycles of reversal loadings were carried out to investigate the behavior of the MFPS base isolator. The test results given in Fig. 6 show that the behavior of the MFPS base isolator during the 228 cycles is very stable. Furthermore, there is no any sign of degradation of the Teflon composite liner coated in the sliding interface from visual inspection. The shear force of the 20^{th} cycle is 92.5% of that of the 1^{st} cycle due to the considerable energy accumulated in the sliding interface. The horizontal stiffness measured 208.287 tons/m from these tests is very close to the theoretical value of 201.252 tons/m, hence, the accuracy of the manufacture of the proposed device can be controlled within a desirable range.

SHAKING TABLE TESTS OF A STEEL STRUCTURE WITH MFPS ISOLATORS

In order to evaluate the effectiveness of the MFPS base isolator on seismic mitigation, the shaking table tests of a full scale steel structure isolated with the proposed isolators were conducted at the National Center for Research on Earthquake Engineering in Taiwan. Typical strong ground motions of the 1940 El Centro earthquake which is usually adopted in shaking table tests have been given as inputs during the tests. Additionally, the near fault and soft-soil-deposit site earthquakes which contain long predominant periods have also been imposed on the base isolated structure to investigate the effectiveness of the proposed device. As shown in Fig. 7, the three-story structure is 9m in height and the total weight of the structure is about 40tons. The properties of columns and girders of the steel structure are $H200 \times 200 \times 8 \times 12$ and $H200 \times 150 \times 6 \times 9$, respectively. In order to increase the rigidity of the superstructure, diagonal steel bracings ($2L100 \times 100 \times 13$) had been installed on the structure during the tests. The MFPS isolator adopted in the shaking table tests has doubled concave surfaces of 2.236m in radius of curvature, and the diameter of the articulated slider is 7.8cm. The comparison of the time history of the roof acceleration response between the bare and base-isolated structures under the uniaxial El Centro earthquake (NS component) of 1.047g in PGA is shown in Fig. 8. It is shown from the table and the figure that significant reductions of seismic responses can be achieved by the installation of the proposed devices. Even during the severe earthquake of 1.047g in PGA, the maximum roof acceleration is merely 0.396g. Hence, the proposed device can be regarded as a powerful tool for upgrading the seismic resistibility under earthquakes. The average hysteresis loop response of the MFPS base isolation system under the El Centro earthquake of 1.047g in PGA is also given in Fig. 8. The friction damping provided by the sliding interface can help to dissipate the accumulated seismic energy, therefore, the maximum sliding displacement is only 13.6cm even subjected to 300% El Centro earthquake. The comparisons of the roof acceleration and the hysteresis loop response of the MFPS isolated structure under the Kobe earthquake are given in Fig. 9. Significant reduction in acceleration response and highly nonlinear behavior of the proposed isolator can be observed in this figure. During the shaking table tests, the severe earthquake of the TCU084 Chi-Chi earthquake of 1.211g in PGA had also been adopted. It is shown from Fig. 10 that the acceleration response of the superstructure can be lessened by using the proposed isolators. Moreover, the efficiency of friction damping on dissipating the seismically accumulated energy can also be shown from the figure.

In recent years, some researchers suspect the efficiency of the base isolation systems under ground motions with long predominant periods. Strong ground motions measured at the Taipei basin, which contain long predominant periods in the range of 1.2~1.6sec, have been adopted in the shaking table tests. In this study, the recorded PGA of 0.076g, 0.0482g and 0.0258g in NS, EW and vertical components of the 2002 Hua-Lien earthquake (TAP098) was scaled up over tenfold of the original to investigate the behavior of a base-isolated structure located at the Taipei basin under severe earthquakes. The experimental results of the roof acceleration and average hysteresis loop are given in Fig. 11. Due to the doubled concave surfaces and the lubricant material, the proposed isolator can easily shift the fundamental period of the structure into the range of 4~5sec with sufficient damping. The maximum floor accelerations under severe earthquakes are mainly in the range of 0.15~0.3g, therefore, the proposed isolator can be adopted as a good tool in mitigating seismic responses of a structure located at a soft-soil-deposit site. The experimental results aforementioned demonstrate that the MFPS base isolator can enhance the seismic resistibility of a structure subjected to an earthquake with long predominant periods.

FINITE ELEMENT FORMULATIONS FOR MFPS BASE ISOLATOR

In order to simulate the nonlinear behavior of the MFPS accurately, as shown in Fig. 12, a two-node finite element has been proposed in this study. As shown in Fig. 13, the element includes a nodal point at the center of the lower concave sliding interface (nodal point 1) and another nodal point at the center of the upper concave sliding interface (nodal point 2). As shown in Fig. 13, the equilibrium equation of the lower concave sliding interface in the vertical direction can be given as:

$$W - P_1 \cos\theta_1 + T_1 \sin\theta_1 = 0 \tag{1}$$

The equilibrium equation in the horizontal direction can be expressed as:

$$F_1 - P_1 \sin\theta_1 - T_1 \cos\theta_1 = 0 \tag{2}$$

where W is the vertical loading resulting from the superstructure; P_1 is the contact force normal to the sliding surface; F_1 is the horizontal force imposing on the lower concave sliding interface; T_1 is the tangent component of the friction force in the $F - W$ plane.

Rearrangement of Eqs. (1) and (2) gives:

$$F_1 = W \tan\theta_1 + \frac{T_1}{\cos\theta_1} = \bar{k}_{r1}\overline{D}_{r1} + \frac{T_1}{\cos\theta_1} \tag{3}$$

where

$$\overline{D}_{r1} = R_1 \sin\theta_1 \tag{4}$$

$$\bar{k}_{r1} = \frac{W}{R_1 \cos\theta_1} \tag{5}$$

in which R_1 is the radius of the lower concave sliding interface.

Similarly, as shown in Fig. 13, the equilibrium equation of the upper concave surface in the vertical and horizontal directions can be shown as:

$$W - P_2 \cos\theta_2 + T_2 \sin\theta_2 = 0 \tag{6}$$

and

$$F_2 - P_2 \sin\theta_2 - T_2 \cos\theta_2 = 0 \tag{7}$$

The solution to Eqs. (6) and (7) is:

$$F_2 = W \tan\theta_2 + \frac{T_2}{\cos\theta_2} = \bar{k}_{r2}\overline{D}_{r2} + \frac{T_2}{\cos\theta_2} \tag{8}$$

in which

$$\overline{D}_{r2} = R_2 \sin\theta_2 \tag{9}$$

$$\bar{k}_{r2} = \frac{W}{R_2 \cos\theta_2} \tag{10}$$

where R_2 is the radius of the upper concave sliding surface.

According to Eqs. (3) and (8), one can obtain the horizontal sliding displacements for the lower and upper concave sliding surfaces:

$$\overline{D}_{r1} = \frac{F_1 - \dfrac{T_1}{\cos\theta_1}}{\bar{k}_{r1}} \tag{11}$$

and

$$\overline{D}_{r2} = \frac{F_2 - \dfrac{T_2}{\cos\theta_2}}{\overline{k}_{r2}} \tag{12}$$

The total sliding displacement, $\overline{D}_r$, is the summation of the sliding displacements of the upper and lower concave surfaces, and can be expressed as:

$$\overline{D}_r = \overline{D}_{r1} + \overline{D}_{r2} = \frac{F_1 - \dfrac{T_1}{\cos\theta_1}}{\overline{k}_{r1}} + \frac{F_2 - \dfrac{T_2}{\cos\theta_2}}{\overline{k}_{r2}} \tag{13}$$

Because of the equilibrium of shear forces imposing on the lower and upper concave sliding surfaces must be held, accordingly, using $F = F_1 = F_2$, Eq. 13 can be rewritten as:

$$F = \frac{\overline{k}_{r1}\overline{k}_{r2}}{\overline{k}_{r1} + \overline{k}_{r2}}\overline{D}_r + \frac{1}{\overline{k}_{r1} + \overline{k}_{r2}}\left(\frac{T_1\overline{k}_{r2}}{\cos\theta_1} + \frac{T_2\overline{k}_{r1}}{\cos\theta_2}\right) \tag{14}$$

The forces acting in the $F-W$ plane have been established. However, the forces in the moving coordinate system should be transformed into the fixed local coordinate system, ξ, ς and η . As shown in Fig. 14, the angle α between the $F-W$ vertical plane and the ς-direction of the local coordinate system can be expressed as:

$$\alpha = \tan^{-1}\left(\frac{\overline{u}_3(t)}{\overline{u}_2(t)}\right) \tag{15}$$

The total sliding displacement of the advanced FPS in the local coordinate system can be given as:

$$\overline{D}_r = \overline{u}_2\cos\alpha + \overline{u}_3\sin\alpha \tag{16}$$

where $\overline{u}_2(t)$ and $\overline{u}_3(t)$ represent the relative displacement between nodal points 1 and 2 in the ς and η directions, respectively.

Backsubstitution of Eq. (16) into Eq. (14) leads to:

$$F = \frac{\overline{k}_{r1}\overline{k}_{r2}}{\overline{k}_{r1} + \overline{k}_{r2}}\left[\overline{u}_2(t)\cos\alpha + \overline{u}_3(t)\sin\alpha\right] + \frac{1}{\overline{k}_{r1} + \overline{k}_{r2}}\left(\frac{T_1\overline{k}_{r2}}{\cos\theta_1} + \frac{T_2\overline{k}_{r1}}{\cos\theta_2}\right) \tag{17}$$

By using the coordinate transformation, the horizontal forces acting in the moving coordinate system (in the $F-W$ plane) can be transformed into the local coordinate system:

$$\overline{F}_2 = F\cos\alpha = \frac{\overline{k}_{r1}\overline{k}_{r2}}{\overline{k}_{r1} + \overline{k}_{r2}}\left[\overline{u}_2(t)\cos^2\alpha + \overline{u}_3(t)\sin\alpha\cos\alpha\right] + \frac{1}{\overline{k}_{r1} + \overline{k}_{r2}}\left(\frac{T_1\overline{k}_{r2}}{\cos\theta_1} + \frac{T_2\overline{k}_{r1}}{\cos\theta_2}\right)\cos\alpha \tag{18}$$

$$\overline{F}_3 = F\sin\alpha = \frac{\overline{k}_{r1}\overline{k}_{r2}}{\overline{k}_{r1} + \overline{k}_{r2}}\left[\overline{u}_2(t)\sin\alpha\cos\alpha + \overline{u}_3(t)\sin^2\alpha\right] + \frac{1}{\overline{k}_{r1} + \overline{k}_{r2}}\left(\frac{T_1\overline{k}_{r2}}{\cos\theta_1} + \frac{T_2\overline{k}_{r1}}{\cos\theta_2}\right)\sin\alpha \tag{19}$$

where $\overline{F}_2$ and $\overline{F}_3$ represent the horizontal forces acting in the ς and η directions, respectively. Because the MFPS base isolator is highly rigid in its vertical direction, therefore, the infinite vertical stiffness has been adopted in numerical analysis.

$$\overline{F}_1 = E_\infty \overline{u}_1(t) \tag{20}$$

where $\overline{u}_1(t)$ is the relative displacement between nodal points 1 and 2 in the vertical direction, E_∞ is the parameter to describe high vertical stiffness of the MFPS base isolator.
Rearrangement of Eqs. (18), (19) and (20) gives:

$$\begin{Bmatrix} \overline{F}_1 \\ \overline{F}_2 \\ \overline{F}_3 \end{Bmatrix} = \begin{bmatrix} E_\infty & 0 & 0 \\ 0 & \dfrac{\overline{k}_{r1}\overline{k}_{r2}}{\overline{k}_{r1}+\overline{k}_{r2}}\cos^2\alpha & \dfrac{\overline{k}_{r1}\overline{k}_{r2}}{\overline{k}_{r1}+\overline{k}_{r2}}\sin\alpha\cos\alpha \\ 0 & \dfrac{\overline{k}_{r1}\overline{k}_{r2}}{\overline{k}_{r1}+\overline{k}_{r2}}\sin\alpha\cos\alpha & \dfrac{\overline{k}_{r1}\overline{k}_{r2}}{\overline{k}_{r1}+\overline{k}_{r2}}\sin^2\alpha \end{bmatrix} \begin{Bmatrix} \overline{u}_1(t) \\ \overline{u}_2(t) \\ \overline{u}_3(t) \end{Bmatrix} + \begin{Bmatrix} 0 \\ \dfrac{1}{\overline{k}_{r1}+\overline{k}_{r2}}\left(\dfrac{T_1\overline{k}_{r2}}{\cos\theta_1}+\dfrac{T_2\overline{k}_{r1}}{\cos\theta_2}\right)\cos\alpha \\ \dfrac{1}{\overline{k}_{r1}+\overline{k}_{r2}}\left(\dfrac{T_1\overline{k}_{r2}}{\cos\theta_1}+\dfrac{T_2\overline{k}_{r1}}{\cos\theta_2}\right)\sin\alpha \end{Bmatrix} \tag{21}$$

By virtue of the principle of virtual work, the forces acting in the F-W plane can be transformed into the global coordinate system.

$$\begin{aligned} \mathbf{F}_W(t) &= \mathbf{B}^T \begin{Bmatrix} \overline{F}_1 \\ \overline{F}_2 \\ \overline{F}_3 \end{Bmatrix} = \mathbf{B}^T \begin{bmatrix} E_\infty & 0 & 0 \\ 0 & \dfrac{\overline{k}_{r1}\overline{k}_{r2}}{\overline{k}_{r1}+\overline{k}_{r2}}\cos^2\alpha & \dfrac{\overline{k}_{r1}\overline{k}_{r2}}{\overline{k}_{r1}+\overline{k}_{r2}}\sin\alpha\cos\alpha \\ 0 & \dfrac{\overline{k}_{r1}\overline{k}_{r2}}{\overline{k}_{r1}+\overline{k}_{r2}}\sin\alpha\cos\alpha & \dfrac{\overline{k}_{r1}\overline{k}_{r2}}{\overline{k}_{r1}+\overline{k}_{r2}}\sin^2\alpha \end{bmatrix} \mathbf{BU}(t) \\ &\quad + \mathbf{B}^T \begin{Bmatrix} 0 \\ \dfrac{1}{\overline{k}_{r1}+\overline{k}_{r2}}\left(\dfrac{T_1\overline{k}_{r2}}{\cos\theta_1}+\dfrac{T_2\overline{k}_{r1}}{\cos\theta_2}\right)\cos\alpha \\ \dfrac{1}{\overline{k}_{r1}+\overline{k}_{r2}}\left(\dfrac{T_1\overline{k}_{r2}}{\cos\theta_1}+\dfrac{T_2\overline{k}_{r1}}{\cos\theta_2}\right)\sin\alpha \end{Bmatrix} \\ &= \mathbf{B}^T\mathbf{K}_r\mathbf{BU}(t) + \mathbf{B}^T\overline{\mathbf{A}}(t) \end{aligned} \tag{22}$$

However, the friction force normal to the F-W plane (as shown in Fig. 15) should also be taken into account[2-4]:

$$\mathbf{F}_G(t) = \mathbf{B}^T\mathbf{K}_r\mathbf{BU}(t) + \mathbf{B}^T\mathbf{S}(t) \tag{23}$$

where

$$\mathbf{S}(t) = \begin{Bmatrix} 0 \\ \dfrac{1}{\bar{k}_{r1}+\bar{k}_{r2}}\left(\dfrac{T_1\bar{k}_{r2}}{\cos\theta_1}+\dfrac{T_2\bar{k}_{r1}}{\cos\theta_2}\right)\cos\alpha - \dfrac{1}{\bar{k}_{r1}+\bar{k}_{r2}}\left(Q_1\bar{k}_{r2}+Q_2\bar{k}_{r1}\right)\sin\alpha \\ \dfrac{1}{\bar{k}_{r1}+\bar{k}_{r2}}\left(\dfrac{T_1\bar{k}_{r2}}{\cos\theta_1}+\dfrac{T_2\bar{k}_{r1}}{\cos\theta_2}\right)\sin\alpha + \dfrac{1}{\bar{k}_{r1}+\bar{k}_{r2}}\left(Q_1\bar{k}_{r2}+Q_2\bar{k}_{r1}\right)\cos\alpha \end{Bmatrix} \tag{24}$$

The comparisons of the roof acceleration response between the experimental and numerical results under the El Centro earthquake are given in Figs. 16 and 17, respectively. It is shown from these figures that very good prediction can be achieved by using the proposed mathematical model. Not only the roof acceleration response can be predicted accurately, but also the highly nonlinear behavior of the MFPS is calculated with good accuracy by using the proposed theory. The comparisons between the acceleration response and hysteresis loop of the MFPS isolated structure under the TAP098 Hua-Lien Earthquake given in Figs. 18 and 19 also demonstrate the accuracy of the proposed formulations.

CONCLUSIONS

In this study, the shaking table and the full scale component tests of a recently proposed isolator called the Multiple Friction Pendulum System have been conducted to investigate its effectiveness and durability. The results from shaking table tests show that the MFPS isolator can mitigate the acceleration response in the range of 70 to 90 percent as compared with that of the bare structure under different types of ground motions. As the base isolated structure subjected to ground motions with long predominant periods, the proposed isolator also possesses an excellent earthquake-proof benefit without significant sliding displacements. The component test results of the Teflon composite and the full scale MFPS isolator reveal that the proposed isolator coated with the new composite behaves very stably during reversal loadings. Furthermore, the mathematical formulations presented in this study can accurately predict the nonlinear behavior of the structure isolated with MFPS isolators. Therefore, it can be concluded that the proposed concepts in theory and engineering practice can be regarded as powerful tools in designing and enhancing seismic resistibility of structures located at various types of foundations.

REFERENCES

(1)V. A. Zayas, S. S. Low and S. A. Mahin (1987), “The FPS Earthquake Resisting System Experimental Report”, Technical Report, UBC/EERC-87/01.

(2)C. S. Tsai , “Seismic behavior of buildings with FPS isolators”, *Second Congress on Computing in Civil Engineering,* ASCE, Atlanta, GA, pp.1203-1211.(1995).

(3)C. S. Tsai , “Finite Element Formulations For Friction Pendulum Seismic Isolation Bearings”, *International Journal For Numerical methods In Engineering*, vol. 40, pp.29-49, (1997).

(4)C. S. Tsai, T. C. Chiang, C. K. Cheng, W. S. Cheng and C. W. Chang (2002) “An Improved FPS Isolator for Seismic Mitigation on Steel Structures”, The 2002 ASME Pressure Vessels and Piping Conference, Vancouver, Canada, Vol. 445-2, 237-244.

(5)Y. P. Wang, L. L. Chung and W. H. Liao, “Seismic Response analysis of Bridges Isolated with Friction Pendulum Behavior”, Earthquake Engineering and Structural Dynamics, 1998, Vol. 27 pp. 1069-1093.

(6)Jose L. Almazan, Juan C. De La Llera and Jose A. Inaudi, “Modelling Aspects of Structures Isolated with the Frictional Pendulum System”, Earthquake Engineering and Structural Dynamics, 1998, pp. 845-867.

(7)C. S. Tsai, T. C. Chiang and B. J. Chen, “Finite Element Formulations and Theoretical sturdy for Variable Friction Pendulum System”, Engineering Structure, 2003, Vlo. 25, pp. 1719-1730.

(8)R. S. Jangid and J. M. Kelly, “Base Isolation for Near-Fault Motions”, Earthquake Engineering and Structural Dynamics, 2001, Vol. 30, pp. 691-707.

(9)C. S. Tsai, T. C. Chiang and B. J. Chen (2003) “Seismic Behavior of MFPS Isolated Structure Under Near-Fault Earthquakes and Strong Ground Motions with Long Predominant Periods” 2003 ASME Pressure Vessels and Piping Conference, Cleveland, Ohio, U. S. A., Vol. 466, Edited by J. C. Chen, 73-79.

(10)C. S. Tsai, T. C. Chiang and B. J. Chen (2003) “Shaking Table Tests of a Full Scale Steel Structure Isolated with MFPS” 2003 ASME Pressure Vessels and Piping Conference, Cleveland, Ohio, U. S. A., Vol. 466, Edited by J. C. Chen, 41-47.

(11)A. S. Mokha,, M. C. Constantinou and A. M. Reinhorn, “Teflon bearing in base isolation. I, Testing”, Journal of Structural Engineering, ASCE, Vol. 116, pp.438-454(1990)

(12)M. C. Constantinou, A. S. Mokha, and A. M. Reinhorn, “Teflon baering in base isolation. II, Modeling”, Journal of Structure Engineering, ASCE, Vol.116, pp.455-474, (1990).

(13)C. S. Tsai “Nonlinear Stress Analysis Techniques-NSAT”, Department of Civil Engineering, Feng Chia University, Taichung, Taiwan, R. O .C..

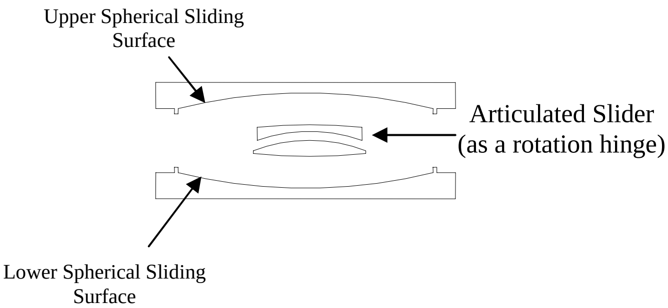

Fig. 1 Cross Section of Multiple Friction Pendulum System

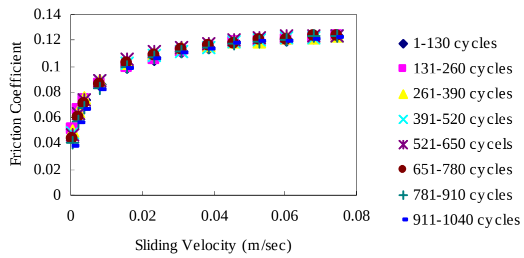

Fig. 3 Friction Coefficient during 1-1040 Reversals

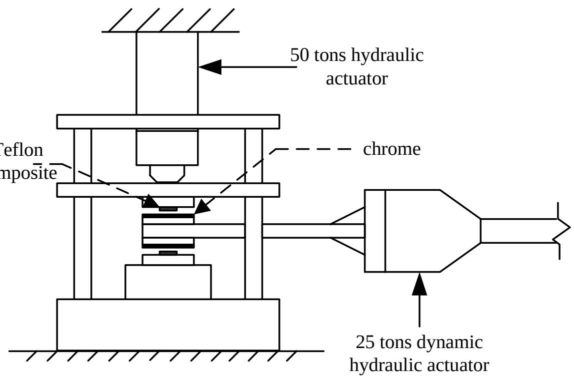

Fig. 2 Test Setup Specimen for Teflon sliding interface

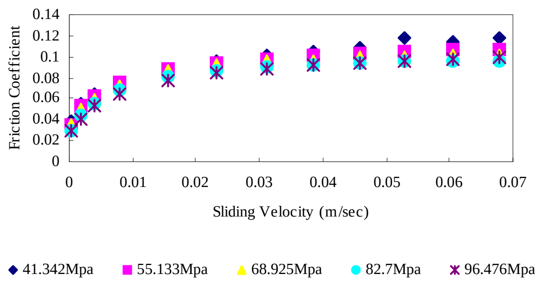

Fig. 4 Relationship between Friction Coefficients and Sliding Velocities under Different Axial Stress

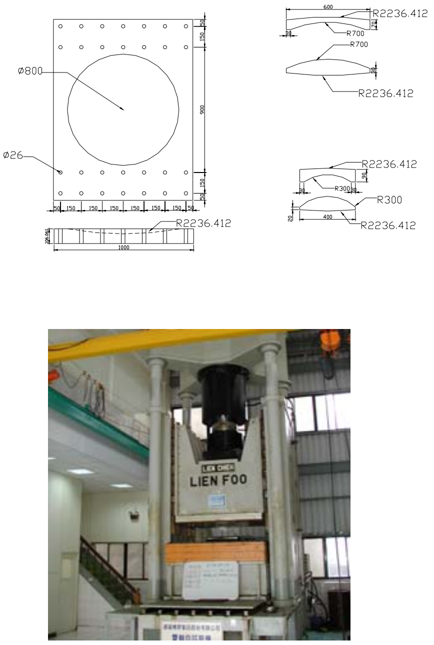

Fig. 5 Specimen and Test Setup for Component Tests

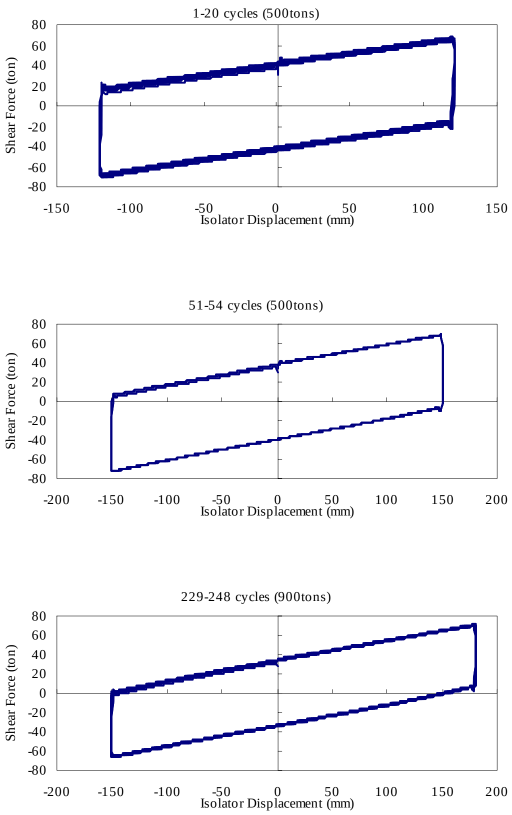

Fig. 6 Force-Displacement Loop for MFPS Base Isolator during Component Tests

Fig. 7 A Full Scale Steel Structure with MFPS Base Isolators

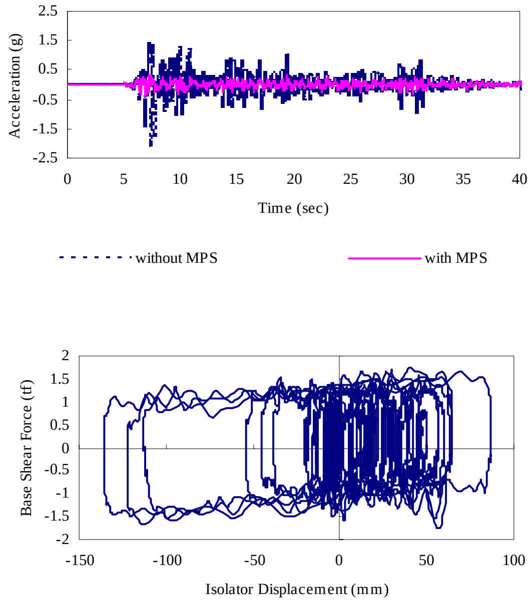

Fig. 8 Roof Acceleration Response and Average Hysteresis Loop of MFPS Base Isolation System in Longitudinal Direction during Uni-axial El Centro Earthquake (NS Component, PGA=1.047g)

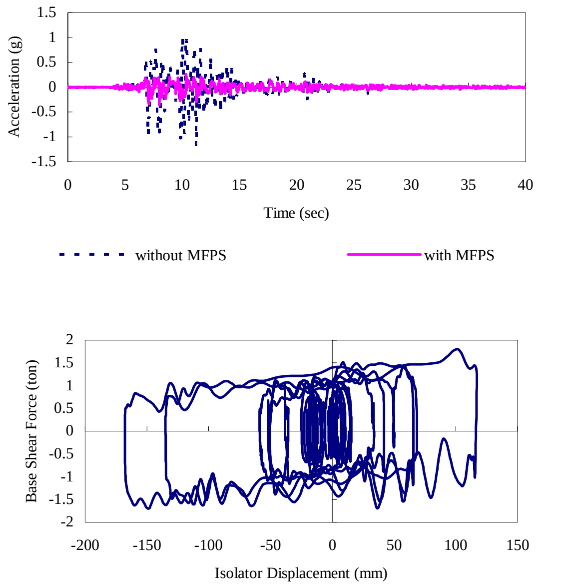

Fig. 9 Roof Acceleration Response and Average Hysteresis Loop of MFPS Base Isolation System in Longitudinal Direction during Kobe Earthquake (NS Component) of 0.858g in PGA

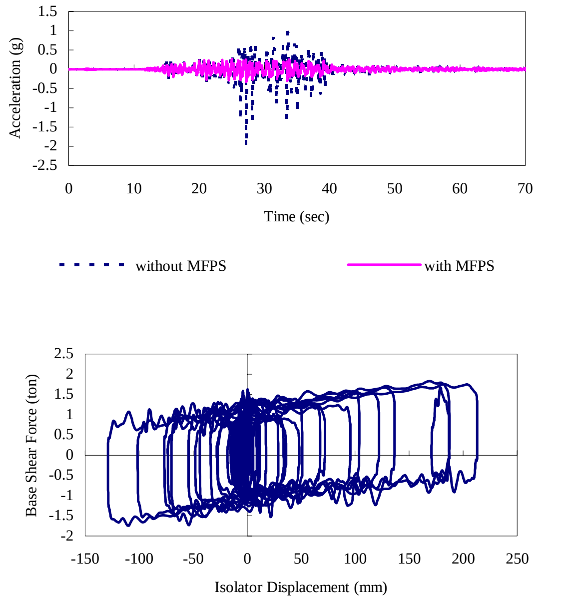

Fig. 10 Roof Acceleration Response and Average Hysteresis Loop of MFPS Base Isolation System in Longitudinal Direction during TCU084 Chi-Chi Earthquake (EW Component) of 1.211g in PGA

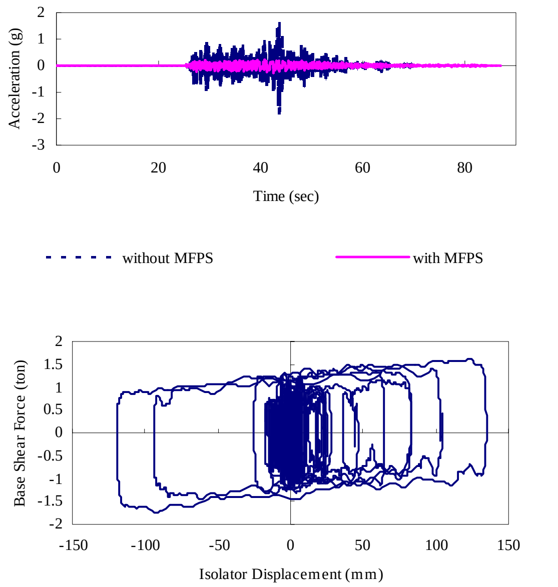

Fig. 11 Roof Acceleration Response and Average Hysteresis Loop of MFPS Base Isolation System in Longitudinal Direction during Hua-Lien Earthquake (NS Component, TAP098) of 1.175g in PGA

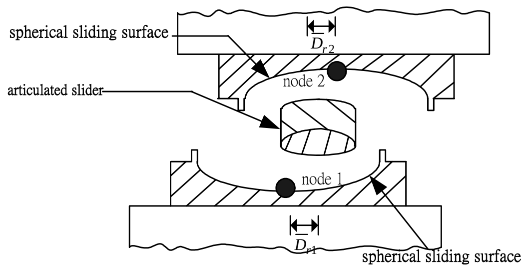

Fig. 12 Two Node Finite Element for MFPS

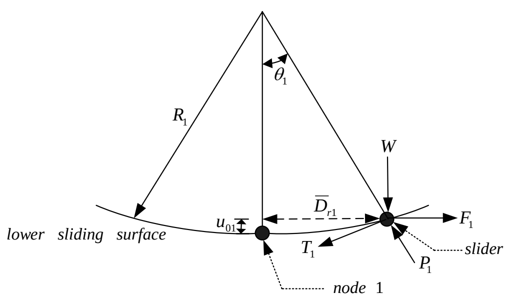

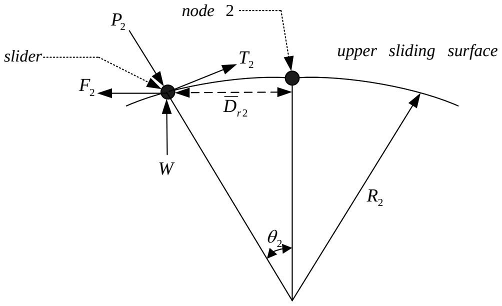

Fig. 13 Forces at Lower and Upper Concave Surfaces

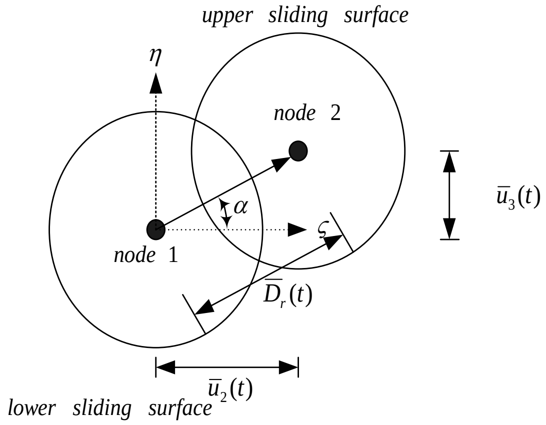

Fig. 14 Top View of Motion of MFPS Isolator

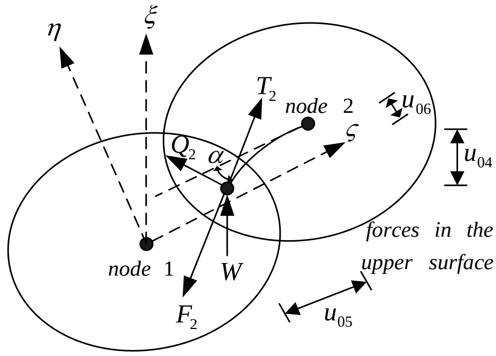

Fig. 15 Forces Acting in F-W Plane

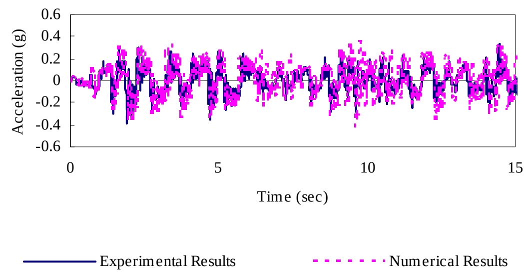

Fig. 16 Comparison of Roof Acceleration under El Centro Earthquake (NS Component PGA=1.047g)

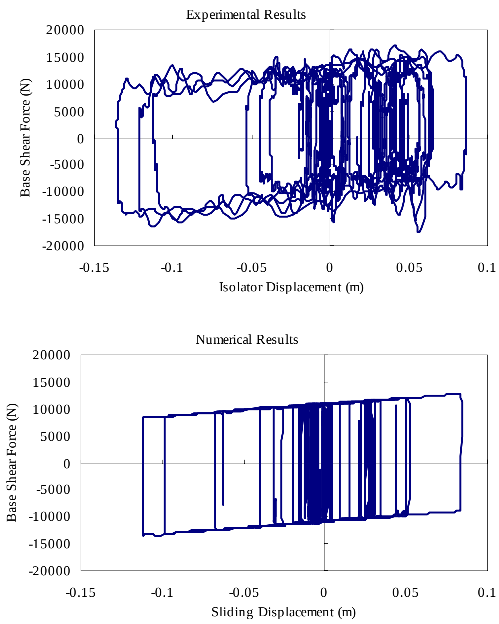

Fig. 17 Comparison of Hysteresis Loop under El Centro Earthquake (NS Component PGA=1.047g)

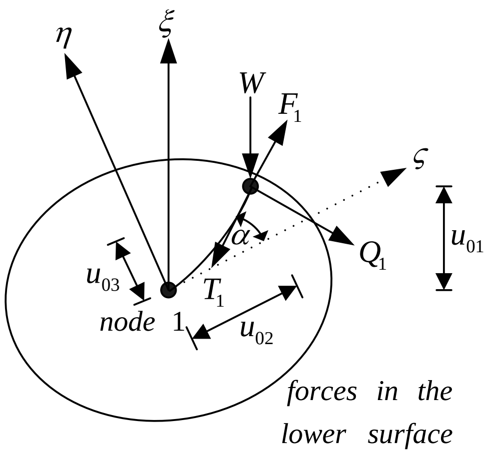

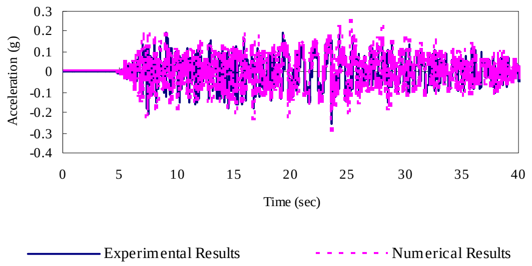

Fig. 18 Comparison of Roof Acceleration under TAP098 Hua-Lien Earthquake (NS Component, PGA=1.175g)

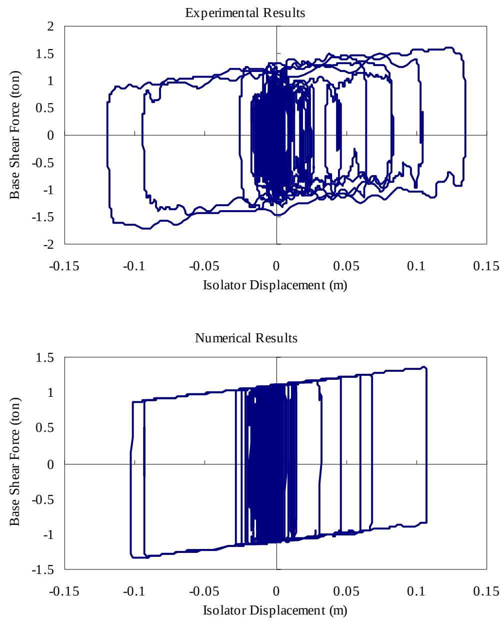

Fig. 19 Comparison of Hysteresis Loop under TAP098 Hua-Lien Earthquake (NS Component, PGA=1.175g)